Alkane Separation

DOI: 10.1002/anie.201205040

Computer-Assisted Screening of Ordered Crystalline Nanoporous Adsorbents for Separation of Alkane Isomers**

David Dubbeldam, Rajamani Krishna, Sofía Calero, and Ahmet Özgür Yazaydın*

The separation of linear, mono-branched, and di-branched isomers of alkanes is of significant importance in the petrochemical industry. For example, the di-branched alkanes in the 5–7 carbon number range are preferred components of high-octane gasoline. Their selective removal from the other isomers produced in an alkane isomerization reactor can be achieved using ordered crystalline nanoporous materials, such as zeolites, metal–organic frameworks (MOFs), covalent organic frameworks (COFs), and zeolitic imidazolate frameworks (ZIFs), by exploiting subtle differences in molecular configurations. Literally, several thousands of such materials have been synthesized, making the choice of adsorbent a daunting task. Our approach is to carry out molecular simulations on a pre-screened list of more than 100 nanoporous structures. Our screening methodology demonstrates that ZIF-77, whose synthesis was reported in 2008,[1] has significantly higher selectivities, by about two orders of magnitude, over other materials that are currently used and for which patents have been issued.

In the petroleum industry, catalytic isomerization is used to convert linear alkanes into their branched isomers.[2] Isomerization processes generate a mixture of isomers that usually require separation and recycling of the non-isomerized components. For example, the effluent of a paraffin isomerization reactor may contain normal alkanes, mono-methyl alkanes and di-methyl alkanes. Traditionally, only the normal alkanes would be separated from the mixture by adsorption (e.g. using the LTA (Linde Type A) type sieve which only adsorbs linear alkanes) and recycled to the isomerization reactor, and any mono-methyl alkanes would be collected with the di-methyl alkanes as product. However, it is the di-methyl alkanes that are the most desired because they have the highest octane numbers. Therefore, a more efficient approach would be to adsorptively separate only the di-methyl alkanes as product and recycle the normal and the mono-methyl alkanes to the isomerization reactor,[3,4] schematically depicted in Figure 1. Ordered crystalline porous materials, such as zeolites, offer the potential for selective adsorption exploiting differences in molecular configurations. Zeolites are readily available, very stable, and cheap. The zeolite should have the right combination of high adsorption selectivity, combined with adequate capacity for use in traditionally used fixed-bed devices. CFI zeolite[5] and ATS zeolite[6] have been suggested for use in this separation in two patents. The undisclosed material in the patents[7,8] is most likely to be MFI-type zeolite.[9] It is of vital importance to improve the energy efficiency of this process to generate more and cleaner gasoline from every barrel of oil.

There has been a recent upsurge in next-generation nanoporous crystalline materials, such as MOFs,[10–15] COFs,[16,17] and ZIFs.[18] There are almost unlimited structural possibilities because of the wide variety of combinations of metal atoms, organic linker molecules, and the building blocks used in self-assembly during synthesis. Each year the synthesis of several hundred new structures is reported and this has created the need to screen these efficiently. There is also a need to understand structure–property relations, such as the mechanisms of alkane separation as a function of shape and size of the pore system. Molecular simulations have sufficiently advanced in both speed and accuracy to allow rapid evaluation of (hypothetical) structures for storage and/or separation devices.[19,20] The first step in our screening procedure is to pre-select, for further examination, only those nanoporous structures that have pore sizes that are large enough to accommodate alkanes molecules with seven or less carbon atoms. After this pre-screening, we performed a complete molecular simulation study on selected structures. The simulation model describes the system in full atomistic detail and is explained in detail in the Supporting Information (Section 1 on modeling and validation of the simulations). The force field we have used produces results in very good agreement with available experimental data and has good predictive capability (see Section 1 Supporting Information). The over one hundred structures we selected from zeolites, MOFs, COFs, and ZIFs provide a broad sample of available nanoporous materials. For each structure we have computed the nC6-2MP-3MP-22DMB-23DMB (nC6 = *n*-hexane, 2MP = 2-methylpentane, 3MP = 3-methylpentane, 22DMB = 2,2-dimetylbutane, 23DMB = 2,3-dimethylbutane) and nC7-2MH-3MH-22DMP-23DMP (nC7 = *n*-heptane, 2MH = 2-methylhexane, 3MH = 3-metylhexane, 22DMP = 2,2-dimethylpentane, 23DMP = 2,3-dimethylpentane) single compo-

[*] Dr. D. Dubbeldam, Prof. Dr. R. Krishna
Van't Hoff Institute for Molecular Sciences, University of Amsterdam
Science Park 904, 1098 XH Amsterdam (The Netherlands)
E-mail: D.Dubbeldam@uva.nl
Homepage: http://molsim.chem.uva.nl
Prof. Dr. S. Calero
Departamento de Sistemas Físicos, Químicos y Naturales, Universidad Pablo de Olavide, Sevilla (Spain)
Dr. A. Ö. Yazaydın
Department of Chemical Engineering, University of Surrey (UK)

[**] This work is supported by the Netherlands Research Council for Chemical Sciences (NWO/CW) through a VIDI grant (D.D.) and by the European Research Council through an ERC Starting Grant (S.C.). A.O.Y. acknowledges a Marie Curie International Reintegration Grant from the European Commission.

Supporting information for this article is available on the WWW under http://dx.doi.org/10.1002/anie.201205040.

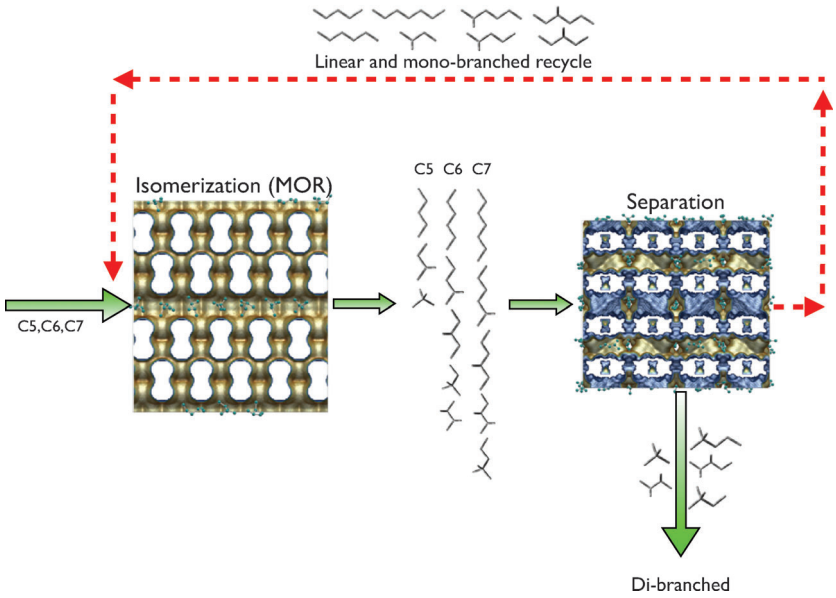

Figure 1. The separation process. The feed consists of mostly linear alkanes. In the first zone (left) linear alkanes are isomerized to branched alkanes, usually using MOR-zeolite which is first converted into the acid form and then acid-leached to increase the silica/alumina ratio. The second zone (right) separates linear and mono-branched (which are recycled back) from the desired di-branched alkanes. Our study focuses on optimizing this separation process.

nent and equimolar mixture isotherms at a typical reactor temperature of 433 K and a wide pressure range. Moreover, we computed surface areas, pore volume, and pore size distributions to relate the results to the pore size and shape. We will denote the order linear ≫ mono-branched ≫ di-branched as "normal hierarchy", and the order di-branched ≫ mono-branched ≫ linear as "reverse hierarchy". For structures that showed significant selectivity, the breakthrough (step-and pulse-style) curves of the nanoporous separation devices were computed.

In the Supporting Information we have compiled the simulation data for each structure (zeolites, MOFs, COFs, and ZIFs in Sections 3, 4, 5, and 6, respectively). Nomenclature and definitions are listed in the Supporting Information. Of all the structures examined, only a handful show an ordered adsorption hierarchy (this "shortlist" is studied in high detail in Section 2 of the Supporting Information). Figure 2 shows the mixture isotherms of highlighted structures: MFI, UiO-66, CoBDP, and ZIF-77. Previous computational studies found high selectivities occurring in MFI zeolite,[9,21,22] and the CoBDP metal–organic framework.[23] Recently, it has been reported (experimentally) that UiO-66 shows reverse shape selectivity: 22DMB = 23DMB > 3MP ≫ nC6.[24] Our simulated mixture isotherms (Figure 2c) as well as the simulated breakthrough for UiO-66 (Supporting information, Figure S6) agree well with this experimental finding. Herein we newly report the use of ZIF-77 for alkane separation, and Figure 2d shows the superior behavior of the ZIF-77 mixture isotherms. In contrast to MFI-zeolite, which has its highest efficiency at pressures that are unlikely to be obtainable in industrial applications, the ZIF-77 can operate efficiently at all pressures.

Figure 3a shows the selectivity of the most promising structures. The simulations appear to provide support of the information in the patent literature about the effectiveness of CFI and MFI zeolites for separation of hexane isomers. However, our simulations show that selectivity improvements by one to two orders of magnitude are possible by use of ZIF-77. Besides selectivity, it is also the capacity of the material that determines the efficiency of a separation device. In pressure swing adsorbers, higher adsorption capacities are desirable because they result in lower frequencies in the regeneration cycles.[25] Figure 3b compares the adsorption selectivity and capacity for various structures. ZIF-77 has not only a much higher adsorption selectivity, but at the same time has a comparable capacity to CFI- and MFI-zeolite. COF-102 and COF-103 have a very high capacity but low adsorption selectivity. The CoBDP and UiO-66 structures are in between; they have moderate selectivities combined with intermediate capacities. To demonstrate the separation potential of ZIF-77 we performed pulse chromatographic simulations. Figure 4 shows ZIF-77 is able to fractionate the components individually on the basis of the degree of branching. None of the other examined structure is able to do this; evidence provided in Supporting Information Figure S17, S24, S31, S38, S45, and S52. Note each component in the mixture seems to behave independently of the type of mixture it is in, as is evidenced by the fact that the breakthrough of the component pulses occurs at the same time, irrespective of whether it is present in a 5-component or 13-component mixture.

To provide insights into the reasons for the differences in selectivities of various structures we performed a systematic study of graphite slits and square channels of varying widths, and carbon nanotubes of different diameters. Graphite slits have been artificially kept at a fixed distance. The channels have been created by intersecting sheets orthogonally with other sheets. From the enthalpy of adsorption at large spacings and low loadings (i.e. this corresponds to the adsorption of a single molecule on a surface), plotted in Figure 5a relative to nC6, we find that natural order of adsorption on a flat surface is the normal hierarchy (see also Sections 8, 9, and 10, Supporting Information). The enthalpies for mono-branched molecules are higher than nC6 and the enthalpies of di-branches are even higher in energy. The normal hierarchy is therefore the order that would be expected and any modifications to the normal order are due to the specific confinement that favors specific molecules. This occurs at confinements around 6–7 Å, where the di-branched molecules fit most snugly because they interact strongly with multiple walls. The spacings of 5 Å and smaller deserve special attention. In this region, there is very strong confinement and size exclusion. In Figure 5b we show that the

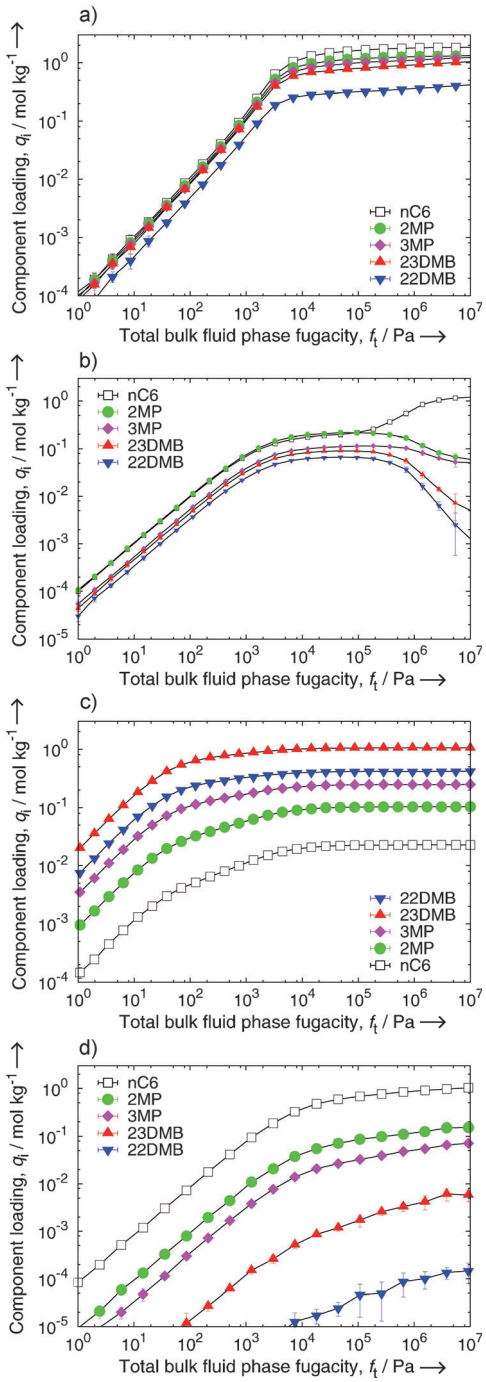

Figure 2. Equimolar mixture isotherms of C6 isomers in a) CoBDP, b) MFI, c) UiO-66, and d) ZIF-77 at 433 K.

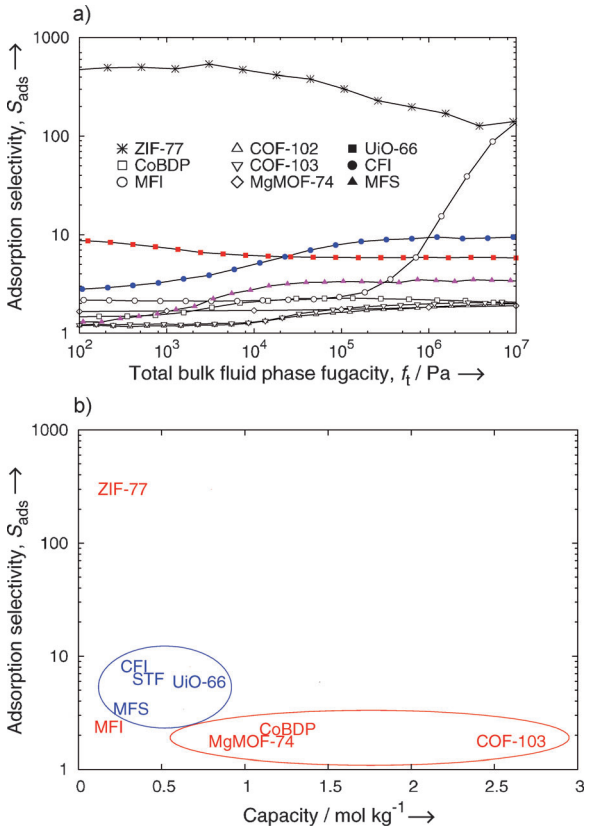

Figure 3. Summary of the screening results: the adsorption selectivity S_{ads}, a) as a function of the total bulk fluid phase fugacity at 433 K, and b) versus capacity for promising structures at 100 kPa. Typical operational reactor pressures are above atmospheric (above 10^5 Pa fugacity). Consider the separation of 5-component hexane isomer mixtures of nC6 (=component 1), 2MP (=component 2), 3MP (=component 3), 23DMB (=component 4), and 22DMB (=component 5) with partial fugacities, f_i, and corresponding loadings, q_i (where i=component number). For materials showing the normal hierarchy (star and open symbols in (a), red in (b)), S_{ads} is defined as $S_{ads}=[(q_1+q_2+q_3)/(q_4+q_5)]/[(f_1+f_2+f_3)/(f_4+f_5)]$, and the capacity as the averaged loadings of linear and mono-branched isomers. For materials with a reverse adsorption hierarchy (closed symbols in (a), blue in (b)), we defined $S_{ads}=[(q_4+q_5)/(q_1+q_2+q_3)]/[(f_4+f_5)/(f_1+f_2+f_3)]$, and capacity as the averaged loadings of the di-branched isomers.

reverse hierarchies we found are all in the 6–7 Å range. Below that range it is possible to have high selectivity (as observed for ZIF-77) owing to strong confinement and size-exclusion, and above the 6–7 Å region we also find the normal hierarchy with lower selectivities. Note that Figure 3b and 5b are qualitatively similar, and spacing and capacity go hand-in-hand. The selectivity is inversely related to spacing.

We have now the necessary information to rationalize the adsorption behavior of hexane isomers as a function of structure. Two hierarchies are possible: the normal hierarchy and the reverse hierarchy. The reverse hierarchy, as observed for UiO-66 and CFI, can only be found in strong-confinement structures and will therefore correspond to structures with relatively small pore volumes. An important disadvantage of the reverse hierarchy is that the hierarchy of the diffusion coefficient is the opposite to the hierarchy of adsorption strengths. The reverse hierarchy structure does show higher selectivities though, but much lower than ZIF-77 and MFI (at very high pressures). In contrast, for the normal adsorption hierarchy the normal hierarchy of diffusivities would enhanced the separation further (e.g. for MFI and ZIF-77). The ZIF-77 has a 2D channel system with larger main channels and smaller side channels. The larger main channels size-exclude the di-branched molecules, while the smaller channels size-exclude the mono- and di-branched. Also of

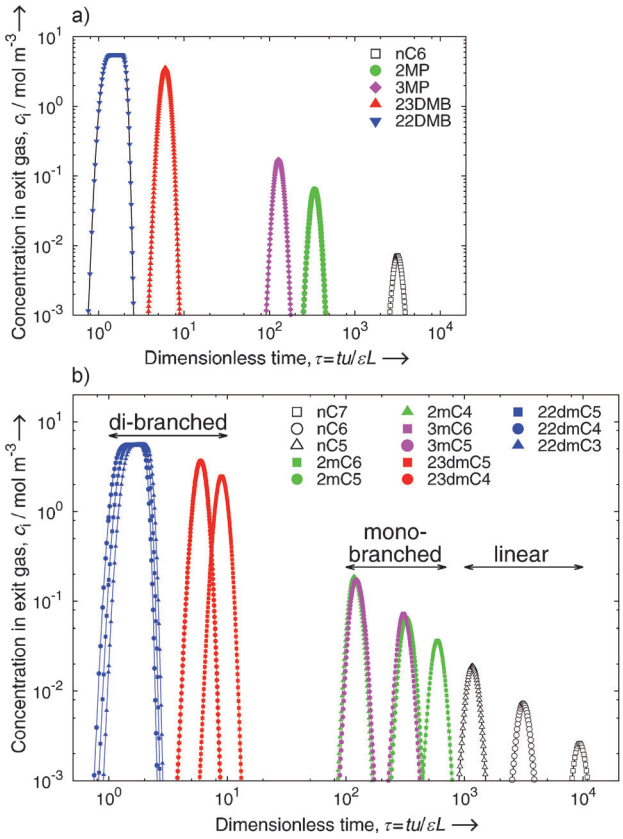

Figure 4. Simulated pulse-style breakthrough curves of a) C6 isomers, b) C5/C6/C7 isomers in ZIF-77 at partial fugacities of the bulk fluid phase of 20 kPa and 433 K. The pulse-style breakthrough clearly shows that ZIF-77 is able to fractionate the individual components of a C6 mixture, and when it is fed an alkane mixture differing in chain length it is still able to fractionate the mixture into linear, mono-branched, and di-branched components. Video animations of the breakthrough behavior as a function of time of ZIF-77 and other selected structures are provided as Supporting Information.

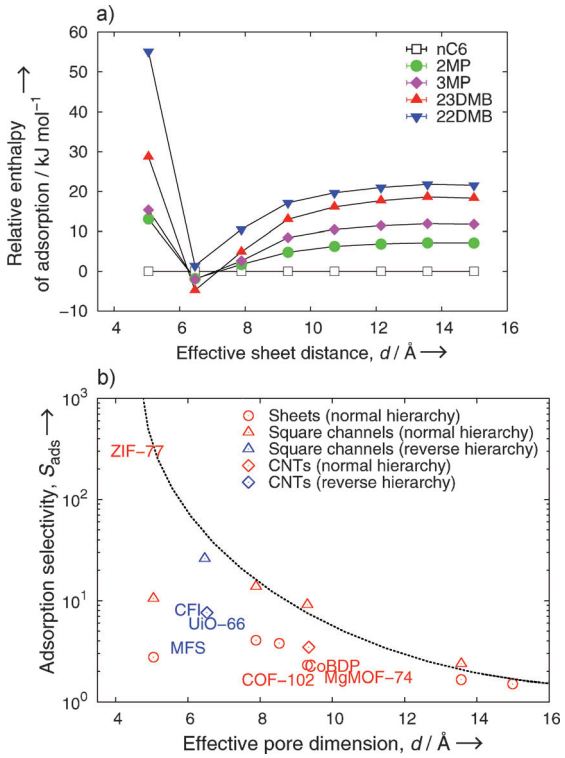

Figure 5. Hexane isomer selectivity at 433 K as a function of confinement, a) enthalpy of adsorption relative to nC6 for graphite square channels at infinite dilution, b) adsorption selectivity at 100 kPa. Red denotes normal hierarchy, blue reverse hierarchy, the dotted line shows the qualitative behavior of the selectivity.

high interest is CoBDP which combines good selectivity with a high pore volume. The qualitative shape of the isotherms at about 9.3 Å (see subsection 8.10 and 9.4 of the Supporting Information) agrees well with the isotherms obtained for the CoBDP structure. As the results for a smaller spacing appear qualitatively better, it seems possible to optimize the CoBDP structure further by making it slightly smaller. The CoBDP channel is corrugated, because of rotation of the linker molecule, and only approximately rectangular and actually a combination of optimal parts with sub-optimal parts. In the Supporting Information (Section 7) we show results for various modifications of a pseudo-version of CoBDP, created using the Materials Studio Visualizer.[26] We have made the structure rectangular and changed the linker molecule BDP (benzenedipyrazolate) to ADP (acetylenedipyrazolate), BP (bipyrazolate), and BPDP (biphenyldipyrazolate). None of these hypothetical structures are significantly better, indicating that it might be non-trivial to reduce or extend the channel dimensions of crystalline materials by altering the organic linker molecules.

Large-pore MOFs do not show significant alkane selectivity; most of the pore-volume is unused and non-selective. Note that in a square channel, all available pore volume is used. The cylindrical channels we studied are known as carbon nanotubes (CNTs). CNTs are unlikely to be as efficient as the square channels owing to the large amount of unused pore volume. As with a square channel, triangular and honeycomb channel systems would also utilize all of the available pore volume. A honeycomb structure can possibly be made from graphene sheets.[27] Other interesting alkane/carbon-framework systems include mesoporous silica with intraporous nanocarbon.[28]

Our discovery of the unique separation capability of the ZIF-77 would not have been unearthed using a conventional screening study based on, for example, pore size distributions. The reason is that the pores of ZIF-77 are highly non-cylindrical. The pore size distribution of ZIF-77 could be wrongly interpreted as that there are no pores larger than 4.5 Å in diameter. However, this is the shortest distance, and in the other direction the pore is much larger. In fact, linear, mono-branched, and 2,3-di-branched alkanes fit in. Simulations were conducted to compute the self-diffusion coefficients at 433 K and infinite dilution. The hierarchy of diffusivities is linear > mono-branched > 2,3-di-branched ≫ 2,2-di-branched. The 2,2-di-branched is too bulky to enter the pore system. It would be challenging to refine currently used conventional screening methods to be able to detect

systems like ZIF-77. But as we show herein, currently it is feasible to analyze over a 100 structures in full detail, and with current advances in computational efficiency, future screenings could handle many, many more structures.

In conclusion, we have rationalized the adsorption behavior of hexane (and heptane) isomers and our screening study provides a thorough understanding. First, it is an ill-advised endeavor to use large-pore MOFs for alkane separations. Above a certain threshold (depending on the alkane chain-length) the excess pore volume just goes to waste. Below the threshold for selectivity, both branching hierarchies are possible, but the one corresponding to the largest pore volume (the normal hierarchy) is probably most efficient, also because adsorption and diffusion selectivity go hand-in-hand. To properly evaluate a structure at least a 5-component mixture is needed, with both the 2,2-di-branched and the 2,3-di-branched included, as these have usually very different behaviors. The simulated breakthrough curves provide the best way of assessing the efficiency of a structure. The efficiency depends on a) the selectivity, and b) the accessible pore volume. CoBDP provides a very good compromise between the two, but the selectivity of ZIF-77 is so high that this sieve fractionates to yield individual pure components. The screening strategy we presented can be applied to other problems, such as, for example, separating alkane mixtures with C_{10}–C_{18} hydrocarbons[29] and xylene isomers.[30]

Methods Section

The adsorption computations of single and multi-components are performed using the configurational-bias Monte Carlo algorithm in the grand-canonical ensemble. The systems are modeled in full atomistic detail using calibrated classical force fields. Periodic boundary conditions are used to extrapolate the finite system results to macroscopic bulk values. We checked for finite size and hysteresis effects and both were found to be negligible. Using the dual-site Langmuir–Freundlich fits of the pure component isotherms, breakthrough calculations were carried out by solving a set of partial differential equations for each of the species in the gas mixture. The molar loadings of the species at any position along the packed bed and at any time are determined from ideal adsorbed solution theory calculations. Video animations of the breakthrough behavior as a function of time of selected structures are provided as Supporting Information.

Received: June 27, 2012
Published online: October 19, 2012

Keywords: adsorption · alkane separation · metal–organic frameworks · molecular simulations · ZIF-77

[1] R. Banerjee, A. Phan, B. Wang, C. Knobler, H. Furukawa, M. O'Keeffe, O. Yaghi, *Science* **2008**, *319*, 939 – 943.
[2] W. Vermeiren, J.-P. Gilson, *Top. Catal.* **2009**, *52*, 1131 – 1161.
[3] S. C. Stem, W. Evans, United States Patent No. 4855529, **1989**.
[4] S. C. Stem, W. Evans, United States Patent No. 4804802, **1989**.
[5] T. Maesen, T. Harris, United States Patent No. 7037422, **2006**.
[6] T. Maesen, T. Harris, United States Patent No. 7029572, **2006**.
[7] H. Dandekar, G. Funk, R. Gillespie, H. Zinnen, C. McGonegal, M. Kojima, S. Hobbs, United States Patent No. 5763730, **1998**.
[8] H. Dandekar, G. Funk, H. Zinnen, United States Patent No. 6069289, **2000**.
[9] S. Calero, B. Smit, R. Krishna, *Phys. Chem. Chem. Phys.* **2001**, *3*, 4390 – 4398.
[10] M. Eddaoudi, J. Kim, N. Rosi, D. Vodak, J. Wachter, M. O'Keeffe, O. Yaghi, *Science* **2002**, *295*, 469 – 472.
[11] O. M. Yaghi, M. O'Keeffe, N. W. Ockwig, H. K. Chae, M. Eddaoudi, J. Kim, *Nature* **2003**, *423*, 705 – 714.
[12] S. Kitagawa, R. Kitaura, S. Noro, *Angew. Chem.* **2004**, *116*, 2388 – 2430; *Angew. Chem. Int. ed.* **2004**, *43*, 2334 – 2375.
[13] R. Q. Snurr, J. T. Hupp, S. T. Nguyen, *AIChE J.* **2004**, *50*, 1090 – 1095.
[14] U. Mueller, M. Schubert, F. Teich, H. Puetter, K. Schierle-Arndt, J. Pastre, *J. Mater. Chem.* **2006**, *16*, 626 – 636.
[15] G. Férey, *Chem. Soc. Rev.* **2008**, *37*, 191 – 214.
[16] A. Côté, A. Benin, N. Ockwig, M. O. A. Matzger, O. Yaghi, *Science* **2005**, *310*, 1166 – 1170.
[17] H. El-Kaderi, J. Hunt, J. Mendoza-Cortés, A. Côté, R. Taylor, M. O'Keeffe, O. Yaghi, *Science* **2007**, *316*, 268 – 272.
[18] K. Park, Z. Ni, A. Côté, J. Choi, R. Huang, F. Uribe-Romo, H. Chae, M. O'Keeffe, O. Yaghi, *Proc. Natl. Acad. Sci. USA* **2006**, *103*, 10186 – 10191.
[19] C. Wilmer, M. Leaf, C. Lee, O. Farha, B. Hauser, J. Hupp, R. Snurr, *Nat. Chem.* **2012**, *4*, 83 – 89.
[20] E. Haldoupis, S. Nair, D. Sholl, *J. Am. Chem. Soc.* **2012**, *134*, 4313 – 4323.
[21] R. Krishna, B. Smit, S. Calero, *Chem. Soc. Rev.* **2002**, *31*, 185 – 194.
[22] R. Krishna, J. van Baten, *Sep. Purif. Technol.* **2007**, *55*, 246 – 255.
[23] R. Krishna, J. van Baten, *Phys. Chem. Chem. Phys.* **2011**, *13*, 10593 – 10616.
[24] P. Bárcia, D. Guimarães, P. Mendes, J. Silva, V. Guillerm, H. Chevreau, C. Serre, A. Rodrigues, *Microporous Mesoporous Mater.* **2011**, *139*, 67 – 73.
[25] R. Krishna, J. Long, *J. Phys. Chem. C* **2011**, *115*, 12941 – 12950.
[26] Accelrys Materials Studio for materials modeling & simulation, http://accelrys.com/products/materials-studio/.
[27] S. Yin, Y. Zhang, J. Kong, C. Zhou, C. Li, X. Lu, J. Ma, F. Boey, X. Chen, *ACS Nano* **2011**, *5*, 3831 – 3838.
[28] F. de Clippel, A. Harkiolakis, X. Ke, T. Vosch, G. Van Tendeloo, G. V. Baron, P. Jacobs, J. F. M. Denayer, B. F. Sels, *Chem. Commun.* **2010**, *46*, 928 – 930.
[29] S. Raghuram, S. Wilcher, *Sep. Sci. Technol.* **1992**, *27*, 1917 – 1954.
[30] D. Peralta, G. Chaplais, A. Simon-Masseron, K. Barthelet, C. Chizallet, A.-G. Quoineaud, G. Pirngruber, *J. Am. Chem. Soc.* **2012**, *134*, 8115 – 8126.

